Single-crystal elasticity of grossular- and almandine-rich garnets to 11 GPa by Brillouin scattering

Fuming Jiang, Sergio Speziale, and Thomas S. Duffy
Department of Geosciences, Princeton University, Princeton, New Jersey, USA

Received 11 March 2004; revised 23 June 2004; accepted 2 August 2004; published 28 October 2004.

[1] The high-pressure elasticity of grossular-rich $Grs_{87}And_9Pyp_2Alm_2$ and almandine-rich $Alm_{72}Pyp_{20}Sps_3Grs_3And_2$ natural garnet single crystals were determined by Brillouin scattering to 11 GPa in a diamond anvil cell. The experiments were carried out using a 16:3:1 methanol-ethanol water mixture as pressure medium. The aggregate moduli as well as their pressure derivatives were obtained by fitting the data to Eulerian finite strain equations. The inversion yields K_{S0} = 165.0 ± 0.9 GPa, G_0 = 104.2 ± 0.3 GPa, $(\partial K_S/\partial P)_{T0}$ = 3.8 ± 0.2, and $(\partial G/\partial P)_0$ = 1.1 ± 0.1 for the grossular-rich composition and K_{S0} = 174.9 ± 1.6 GPa, G_0 = 95.6 ± 0.5 GPa, $(\partial K_S/\partial P)_{T0}$ = 4.7 ± 0.3, and $(\partial G/\partial P)_0$ = 1.4 ± 0.1 for the almandine-rich garnet. Both individual and aggregate elastic moduli of the two garnets define nearly linear modulus pressure trends. The elastic anisotropy of the garnets increases weakly in magnitude with compression. Isothermal compression curves derived from our results are generally consistent with static compression data under hydrostatic conditions, and the effects of nonhydrostaticity on previous diffraction data can be identified. The pressure derivatives obtained here are generally lower than those reported in high-pressure polycrystalline ultrasonic elasticity studies. In combination with earlier Brillouin scattering data for pyrope, our results allow us to constrain the effect on elastic moduli of Fe^{2+}-Mg^{2+} substitution in pyrope-almandine, Ca^{2+}-Mg^{2+} in pyrope-grossular, and Fe^{3+}-Al^{3+} substitution in andradite-grossular at high pressures. This new data set thus allows us to place improved constraints on the compositional dependence of seismic velocities in the rocks of the upper mantle. *INDEX TERMS:* 3909 Mineral Physics: Elasticity and anelasticity; 3924 Mineral Physics: High-pressure behavior; 3934 Mineral Physics: Optical, infrared, and Raman spectroscopy; 3919 Mineral Physics: Equations of state; *KEYWORDS:* elasticity, garnet, high pressure, diamond anvil cell, sound velocity, Brillouin scattering

Citation: Jiang, F., S. Speziale, and T. S. Duffy (2004), Single-crystal elasticity of grossular- and almandine-rich garnets to 11 GPa by Brillouin scattering, *J. Geophys. Res.*, *109*, B10210, doi:10.1029/2004JB003081.

1. Introduction

[2] Garnets are abundant minerals in the igneous and metamorphic rocks of the Earth's crust as well as important constituents of the mantle. Natural garnets in peridotites at pressures greater than ~1.5 GPa (45 km depth) in the Earth's mantle are pyrope-rich with variable amounts of grossular and almandine [*Rickwood et al.*, 1968; *Lee*, 2003]. One of the major phase changes expected under upper mantle conditions is the dissolution of pyroxene into the garnet structure producing Al-deficient garnets (majorite) that are stable to the base of the upper mantle [*Ringwood*, 1967, 1991; *Fei and Bertka*, 1999]. Mantle mineralogical models such as pyrolite and piclogite contain garnet volume fractions at low pressures of ~15% and ~22% respectively and these increase to 40% or more vol. fraction of garnet-majorite at transition zone conditions [*Ringwood*, 1991; *Fei and Bertka*, 1999]. For MORB compositions, the garnet fraction ranges from ~25% at conditions corresponding to the top of the upper mantle to ~90% majorite-garnet at transition zone conditions [*Irifune and Ringwood*, 1993]. Understanding the elastic properties of garnets is thus essential to the interpretation of regional seismic profiles of the upper 660 km of the Earth's interior [*Duffy and Anderson*, 1989; *Weidner and Wang*, 2000]. In addition, the effect of compositional changes on elastic properties is important for interpreting lateral variations in seismic velocity imaged by seismic tomography. The effects of Mg^{2+}-Ca^{2+} and Mg^{2+}-Fe^{2+} substitution on the elastic properties of mantle minerals at upper mantle conditions are not well constrained [*Karato and Karki*, 2001]. Such data are necessary, for example, in interpreting seismic and geodynamic studies of the continental lithosphere (tectosphere) in terms of thermal and chemical properties of the region [*Jordan*, 1978; *Forte and Perry*, 2000; *Lee*, 2003]. The

0148-0227/04/2004JB003081$09.00

Table 1. Result of Microprobe and Powder X-Ray Diffraction Analysis at Ambient Conditions[a]

	Oxides, wt %							
	SiO_2	TiO_2	Al_2O_3	FeO	MnO	MgO	CaO	Lattice Parameter, Å
Grossular-rich garnet: $Grs_{87}And_9Pyp_2Alm_1$; other trace; ρ = 3.605 g/cm^3	40.67	0.39	21.35	3.69	0.08	0.67	36.93	11.886
Almandine-rich garnet: $Alm_{72}Pyp_{20}Sps_3Grs_3And_2$; other trace; ρ = 4.132 g/cm^3	37.76	0.01	21.69	33.53	1.39	4.99	1.79	11.536

[a]All iron assumed to be FeO.

elastic properties of garnets are also important for modeling seismic velocities in the lower continental crust [*Jackson et al.*, 1990; *Morozov et al.*, 2003].

[3] The silicate garnet group $X_3Y_2(SiO_4)_3$ includes a series of isostructural species with space group $Ia\bar{3}d$, where the eight coordinated X-site houses cations such as Ca^{2+}, Mg^{2+}, Fe^{2+} or Mn^{2+} and the six coordinated Y-site incorporates Al^{3+}, Fe^{3+} and Cr^{3+} among others. The structure consists of alternating SiO_4 tetrahedra and YO_6 octahedra which share corners to form a three-dimensional network. The elastic tensor for cubic garnets consists of three independent elastic stiffness coefficients: C_{11}, C_{12}, and C_{44}. The bulk moduli of garnets at ambient pressure can be described by elasticity systematics [*Bass*, 1986; *Wang and Ji*, 2001], and can also be related to the relative compressibility of different structural units, especially the dodecahedral site [*Milman et al.*, 2001]. However, a complete picture of the compositional dependence on the shear modulus, individual C_{ij}s, and all pressure derivatives is not yet available [e.g., *O'Neill et al.*, 1989; *Wang and Ji*, 2001].

[4] Owing to their wide compositional range and the ready availability of good quality specimens, the elastic properties of garnets have been studied far more extensively than any other mineral group [e.g., *Wang and Ji*, 2001]. Numerous X-ray diffraction studies at high pressure have reported the isothermal bulk modulus, K_{T0}, and its pressure derivative, $(\partial K_T/\partial P)_{T0}$ [*Knittle*, 1995]. Measurements of the elastic tensor (and corresponding aggregate bulk and shear moduli) at ambient and high pressures have been reported using ultrasonic interferometry or resonant ultrasound spectroscopy as well as light scattering methods such as Brillouin spectroscopy. At ambient pressure, there is good agreement for both individual and aggregate elastic properties among various studies using different experimental techniques. At high pressures, however, there are disagreements of up to 50% or more in reported pressure derivatives of the bulk and shear modulus for a given composition. For example, reported pressure derivatives for the bulk modulus of grossular range from 4.5 [*Weaver et al.*, 1976] to 6.1 [*Olijnyk et al.*, 1991]. Similarly values of $K'_{T0} = (\partial K_T/\partial P)_{T0}$ and $G'_0 = (\partial G/\partial P)_0$ for majorite garnets differ by 60% and 36% in two reported studies [*Gwanmesia et al.*, 1998; *Sinogeikin and Bass*, 2002]. The magnitude of these discrepancies greatly hinders efforts to make geological interpretations on the basis of seismic data [*Sinogeikin and Bass*, 2002].

[5] In this study, we have carried out single-crystal elasticity measurements on grossular-rich ($Ca_3Al_2Si_3O_{12}$), and Fe-rich almandine-pyrope ($(Fe,Mg)_3Al_2Si_3O_{12}$) garnets to pressures in excess of 11 GPa by Brillouin spectroscopy. We have paid careful attention to sources of systematic error (e.g., vignetting due to the limited angular opening of DAC, resulting in asymmetric Brillouin peak lineshape), compositional heterogeneity, and have maintained hydrostatic conditions in the diamond anvil cell. Together with our detailed study on andradite [*Jiang et al.*, 2004] and a previous Brillouin study on pyrope [*Sinogeikin and Bass*, 2000], we are able to constrain the effects of Fe^{2+}-Mg^{2+}, Ca^{2+}%-Mg^{2+}, and Fe^{3+}-Al^{3+} substitution on the elastic properties of garnets at high pressures. Grossular and almandine-rich garnets were chosen because these compositions have not been extensively studied using optical spectroscopy techniques [cf. *Chai et al.*, 1997; *Conrad et al.*, 1999]. Better characterization of such compositions is needed as natural garnets from mantle peridotites contain roughly 12–26 mol % almandine and 2–20 mol % grossular, in addition to 60–86 mol % pyrope [*Rickwood et al.*, 1968; *Lee*, 2003]. Furthermore, we evaluate the cause of the wide variability of the reported pressure derivatives of the elastic moduli among garnets, and derive a consistent set of elastic properties based on optical spectroscopy (Brillouin scattering) studies.

2. Experimental Procedure

[6] A grossular single crystal from Sierra de las Cruces, Coahuila, Mexico and a natural almandine single crystal of

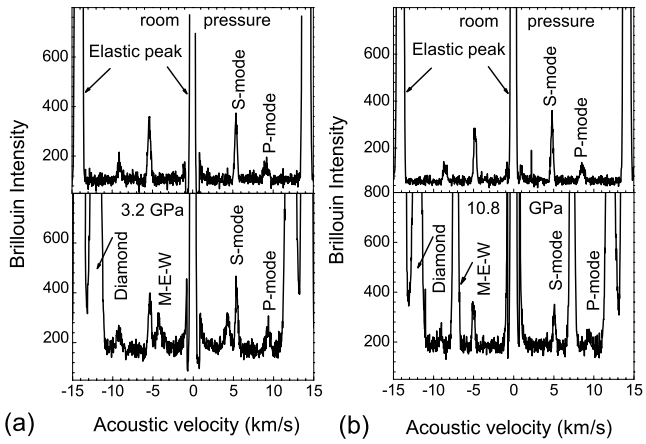

Figure 1. (a) Brillouin spectra of grossular-rich garnet at room pressure and 3.2 GPa. (b) Brillouin spectra of almandine-rich garnet at room pressure and 10.8 GPa. Brillouin peaks from P-mode, S-mode, pressure medium (M-E-W), and diamond are labeled.

Table 2. Best-Fit Density, Elastic Constants, and Aggregate Moduli[a]

P, GPa	ρ, g/cm^3	C_{11}, GPa	C_{12}, GPa	C_{44}, GPa	K_S, GPa	G, GPa	RMS, m/s
			Grossular-Rich Garnet: $Grs_{87}And_9Pyp_2Alm_1$[b]				
0.0001	3.605	314.5(4)	91.5(5)	99.7(2)	165.8(5)	104.3(3)	21
1.6	3.640	323.5(12)	95.1(9)	100.7(5)	171.2(10)	105.9(8)	41
3.2	3.674	332.7(6)	99.9(6)	103.1(3)	177.5(6)	108.2(5)	27
4.3	3.697	337.4(7)	101.7(7)	102.1(3)	180.3(7)	108.1(6)	28
6.5	3.740	352.4(10)	108.6(9)	104.9(5)	189.8(9)	111.4(8)	35
7.9	3.767	354.4(12)	110.7(8)	105.8(4)	191.9(9)	112.0(7)	33
9.4	3.798	370.6(13)	116.6(9)	107.1(5)	201.3(10)	114.7(8)	37
10.7	3.823	377.3(11)	121.3(8)	107.9(5)	206.7(9)	115.5(8)	32
			Almandine-Rich Garnet: $Alm_{72}Pyp_{20}Sps_3Grs_3And_2$[c]				
0.0001	4.132	302.3(4)	110.6(4)	94.4(2)	174.5(4)	94.9(8)	16
1.0	4.155	307.0(10)	109.5(8)	94.4(4)	175.3(9)	96.1(7)	36
2.4	4.187	321.6(11)	121.4(8)	97.8(4)	188.1(9)	98.7(7)	34
3.0	4.200	329.3(8)	124.6(6)	99.5(8)	192.9(7)	100.6(5)	30
5.8	4.263	343.8(9)	130.1(6)	102.8(8)	201.3(7)	104.4(6)	27
7.7	4.303	354.6(9)	137.6(7)	104.9(4)	209.9(8)	106.3(7)	31
9.2	4.333	360.1(10)	140.8(7)	105.6(4)	213.9(8)	107.2(7)	29
10.8	4.364	374.9(8)	150.7(5)	107.7(8)	225.4(6)	109.4(5)	21
12.0	4.388	379.2(17)	152.6(12)	108.6(6)	228.1(14)	110.4(11)	46

[a]Numbers in parentheses are 1-σ deviations in last digit. RMS, root mean square of the difference between observed and calculated velocities.
[b]Average $(\theta_0, \varphi_0, \chi_0) \sim (135° \pm 3, 109° \pm 3, 85° \pm 3)$; $(h\ k\ l) \sim (0.32, 0.95, 1.00)$.
[c]Average $(\theta_0, \varphi_0, \chi_0) \sim (43° \pm 2, -2° \pm 2, 103° \pm 2)$; $(h\ k\ l) \sim (0.22, 0.91, 1.00)$.

unknown origin were used. Both showed characteristic dodecahedral habits. Platelets parallel to the natural {110} faces were cut and then double-side polished with successively finer grits down to a final diamond paper of 1 μm particle size. The final sample thickness was approximately 30 μm. The polished samples were checked using a polarizing microscope, and there was no evidence of zoning. The compositions of the samples used for our Brillouin measurements were determined by electron microprobe analysis. Ten points were analyzed across the samples, and they have equivalent compositions within experimental uncertainties. The densities at ambient conditions were determined by powder X-ray diffraction and chemical analysis (see Table 1).

[7] The polished platelets of grossular- and almandine-rich garnets were loaded into a modified Merrill-Basset diamond anvil cell with angular opening of 96° and compressed up to 11–12 GPa using a 16:3:1 methanol-ethanol-water mixture as a pressure-transmitting medium. In all experiments more than four ruby chips were placed around the sample as pressure calibrants. Pressure determination was performed by measuring the ruby fluorescence shift [*Mao et al.*, 1986]. The fluorescence peaks did not show significant broadening over the whole pressure range. In order to allow for possible stress relaxation after each compression step, Brillouin measurements were carried out at least one day after pressure increase. The differences between pressure measured from different ruby chips around the samples never exceeded ±0.2 GPa. Pressures measured before and after each Brillouin data set collection were always equivalent within mutual uncertainties.

[8] The samples were excited with a single mode vertically polarized neodymium vanadate laser (λ = 532.15 nm) with a power of 150 mW. Brillouin spectra were measured using a six-pass Sandercock tandem Fabry-Perot interferometer in a forward symmetric scattering geometry, in which acoustic velocities, V, can be determined without knowledge of the sample refractive index [*Whitfield et al.*, 1976]:

$$V = \frac{\Delta\nu_B \lambda_0}{2\sin(\theta/2)}, \tag{1}$$

where, λ_0 is the incident laser wavelength, $\Delta\nu_B$ is the measured Brillouin frequency shift and θ is the scattering angle external to the diamond cell (70° in this study). Details of the experimental setup are reported elsewhere [*Speziale and Duffy*, 2002].

[9] Special attention was paid to determine the scattering angle to within a few minutes of a degree using a reference laser beam. Therefore experimental errors due to scattering angles are neglected in our data analysis. The accuracy and reproducibility of our system was tested on standard single crystals of MgO and $SrTiO_3$ with known velocities. A

Table 3. Thermodynamic Parameters Used for Adiabatic to Isothermal Conversion

Parameters	Value	References
	Grossular	
Thermal expansion α_0	19.2×10^{-6} K^{-1}	*Isaak et al.* [1992]
Grüneisen parameter γ_0	1.22	calculated[a]
Specific heat C_P	325.5(7) J/(mol · K)	*Isaak et al.* [1992]
$(\partial K_T/\partial T)_P$	−0.02 GPa · K^{-1}	*Isaak et al.* [1992]
	Almandine	
Grüneisen parameter γ_0	1.22	*Soga* [1967]
$(\partial K_S/\partial T)_P$	−0.0201 GPa · K^{-1}	*Soga* [1967]
$(\partial\alpha/\partial T)_P$	5.24×10^{-8} K^{-2}	*Skinner* [1966]
$(\partial K_T/\partial T)_P$	−0.0277 GPa · K^{-1}	calculated[b]

[a]Grüneisen parameter obtained as $\gamma_0 = \alpha_0 K_{S0}/(\rho_0 C_P)$ using K_{S0} and ρ_0 of this study.
[b]Calculated using $(\partial K_T/\partial T)_P \approx (\partial K_S/\partial T)_P/(1 + \alpha\gamma T) - K_S/(1 + \alpha\gamma T)^2 [\alpha\gamma + (\partial\alpha/\partial T)_P \gamma T]$.

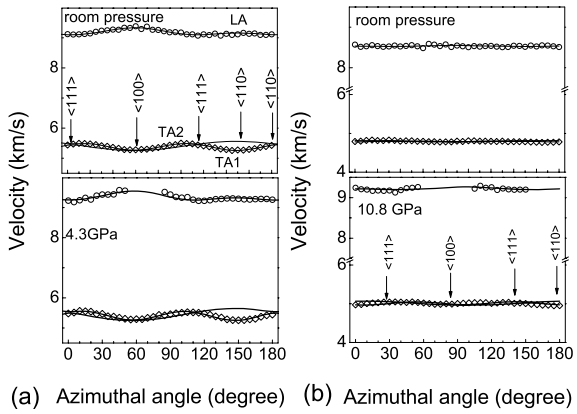

Figure 2. (a) Velocity data (symbols) and calculated velocity curves (lines) of grossular at room pressure and 4.3 GPa. (b) Velocity data and calculated velocity curves of natural almandine at room pressure and 10.8 GPa. Approximate directions [111], [100], and [110] are marked.

significant error in velocity determination can be caused by vignetting due to the limited aperture of the DAC [*Sinogeikin and Bass*, 2000]. To prevent this, a diaphragm was added in front of the collection lens. A half-wave plate in the incident light path was used to maximize the intensity of the Brillouin peaks [*Jiang et al.*, 2004].

3. Results

[10] For all Brillouin spectra, one quasi-longitudinal (P) and one quasi-transverse (S) acoustic mode were observed. Typical Brillouin spectra at ambient and high pressure are shown in Figure 1. The measured frequency shifts have been converted to velocity along the horizontal axis using equation (1). For both samples at each pressure, Brillouin measurement was performed for 36 directions at 5 degree intervals. Eulerian angles (θ_0, φ, χ_0) relating the crystallographic coordinate system to the laboratory coordinate system were used to specify the crystal orientation and acoustic wave-vector direction. The azimuthal angle, φ, was the only one varied during measurement.

[11] The velocity data were fitted to the Christoffel's equation [*Every*, 1980] to retrieve the elastic constants (C_{11}, C_{12}, and C_{44}) and the three Eulerian angles describing the crystal orientation. A starting model based on literature values of C_{ij} and our measured density at ambient conditions was used for the room pressure velocity fitting, and the initial values for θ_0, φ_0, χ_0 were systematically varied until a satisfactory agreement between calculated and experimentally obtained velocities was attained. The recovered orientation indicated that the crystal plane was close to {110} as expected (see Table 2). Despite the very low elastic anisotropy of these garnets ($A = 2C_{44}/(C_{11}-C_{12}) = 0.98$) at ambient pressure for the almandine-pyrope garnet), we found that the crystal orientation could be readily recovered to within ±3 degrees. Densities at high pressures were initially estimated by using the Birch-Murnaghan equation of state, with ambient pressure values of the bulk modulus, K_{T0}, and an initial guess for the pressure derivative of the bulk modulus, $(\partial K_T/\partial P)_{T0}$. High-pressure elastic constants were obtained by fitting each velocity curve using the calculated density and the C_{ij} values from the previous pressure as initial guesses. Errors in pressure determination in turn cause uncertainties in elastic moduli at high pressures by introducing errors in density. Our estimations show that the errors in elastic moduli would be 1.5 times the standard deviation 1-σ given in this study if this error in pressure determination is considered.

[12] After the first round of fitting, the adiabatic aggregate bulk modulus and the aggregate shear modulus, G, obtained from Voigt-Reuss-Hill average, were calculated. In the inversion of high-pressure moduli, an iterative procedure [*Zha et al.*, 1996; *Speziale and Duffy*, 2002] was adopted. The calculated adiabatic bulk moduli K_S were fit to third-order Eulerian finite strain equation [*Birch*, 1978] to obtain K_{S0} and $(\partial K_S/\partial P)_{T0}$. These parameters were then converted to isothermal K_{T0} and $(\partial K_T/\partial P)_{T0}$, by applying thermodynamic relations:

$$K_{T0} = K_{S0}/(1 + \alpha\gamma T) \tag{2}$$

$$(\partial K_T/\partial P)_{T0} \approx (1 + \alpha\gamma T)^{-1}\left[(\partial K_S/\partial P)_{T0} - \gamma T/K_{T0}(\partial K_T/\partial T)_{P0}\right], \tag{3}$$

where α is the volume thermal expansion coefficient and γ is the Grüneisen parameter (Table 3). The isothermal K_{T0} and $(\partial K_T/\partial P)_{T0}$ were then used to construct improved isothermal compression curves and the velocities at each pressure were refit. The above procedure was repeated and it converged after four iterations. It should be mentioned here that the initial values of K_{T0} and $(\partial K_T/\partial P)_{T0}$, which were used to calculate the initial densities at high pressures, did not affect final results, but only affect the number of iterations needed to achieve convergence.

Table 4. Individual Elastic Constants and Pressure Derivatives of Grossular at Ambient Conditions[a]

Study[b]	Composition	C_{11}, GPa	C_{12}, GPa	C_{44}, GPa	$(\partial C_{11}/\partial P)_0$	$(\partial C_{12}/\partial P)_0$	$(\partial C_{44}/\partial P)_0$	P_{max}, GPa
a	$Grs_{87}And_9Pyp_2Alm_1$	313.6(16)	90.7(7)	99.5(4)	6.1(2)	2.8(1)	0.9(1)	11
b	$Grs_{99}And_1$	321.7(8)	91.4(9)	104.6(4)				10^{-4}
c	$Grs_{80}And_{14}Alm_3Pyp_2$	306.1(38)	88.7(38)	98.8(4)				10^{-4}
d	$Grs_{97}And_2Pyp_1$	318.8(8)	92.1(7)	102.9(2)				10^{-4}

[a]Numbers in parentheses are 1-σ deviations in last digit.
[b]Studies are as follows: a, this study; b, *Bass* [1989]; c, *Babuska et al.* [1978]; d, *Isaak et al.* [1992].

Table 5. Aggregated Moduli and Pressure Derivatives of Grossular at Ambient Conditions[a]

Study[b]	Composition	K_{S0}, GPa	K_{T0}, GPa	G_0, GPa	$(\partial K_S/\partial P)_{T0}$	$(\partial K_T/\partial P)_{T0}$	$(\partial G/\partial P)_0$	P_{max}, GPa	Method[c]
a	$Grs_{87}And_9Pyp_2Alm_1$	165.0(9)	163.8(5)	104.2(3)	3.8(2)	3.9(2)	1.1(1)	11	BS
b	$Grs_{99}And_1$	168.4(7)		108.9(4)				10^{-4}	BS
c	$Grs_{80}And_{14}Alm_3Pyp_2$	161.2(5)		120.6(4)				10^{-4}	U
d	$Grs_{97}And_2Pyp_1$	167.8(7)		106.9(2)				10^{-4}	R
e	Grs_{100}	166.8[d]		108.9[d]	5.46		1.10	10	BS
f	$Grs_{90}Pyp_1Alm_2And_6$		173(2)			4.25[d]		25	X
f			162(3)			5.45[d]		25	X
f	$Grs_{97}Sps_1Alm_1$		175(4)			4.25[d]		25	X
f			165(4)			5.45[d]		25	X
g	Grs_{100}		168(25)			6.1(15)		18.4	X
h	$Grs_{97}Alm_3$		169.3(12)			5.92(14)		36.9	X
i	Grs_{100}		175(1)			4.4[d]		11.6	X

[a]Numbers in parentheses are 1-σ deviations in last digit.
[b]Studies are as follows: a, this study; b, *Bass* [1989]; c, *Babuska et al.* [1978]; d, *Isaak et al.* [1992]; e, *Conrad et al.* [1999]; f, *Weaver et al.* [1976]; g, *Olijnyk et al.* [1991]; h, *Pavese et al.* [2001]; i, *Zhang et al.* [1999].
[c]BS, Brillouin scattering; R, resonance method; U, polycrystalline ultrasonic method; X, X-ray diffraction.
[d]Fixed value.

[13] The robustness of our fitting results was confirmed on a standard sample of MgO and also demonstrated by low root mean square (RMS) differences between observed and calculated velocities (Table 2). Figures 2a and 2b show the observed velocities (symbols) and calculated velocity curves (lines) for grossular-rich and almandine-rich crystals at room and high pressure.

4. Discussion

4.1. Elastic Stiffness Constants, Aggregate Moduli, and Their Pressure Derivatives

[14] The adiabatic aggregate bulk moduli, K_S, were fit to Eulerain finite strain equation to obtain K_{S0} and $K'_{S0} = (\partial K_S/\partial P)_{T0}$. They were converted to isothermal values of K_{T0} and K'_{T0} using equations (2) and (3). Pressure derivatives of individual elastic constants C_{ij} and the shear modulus, G, were obtained by fitting experimental values to the third-order finite strain equations [*Davies*, 1974]:

$$C_{ijkl} = (1+2f)^{7/2}\left[C^0_{ijkl} + a_1 f + ..\right] - P\Delta_{ijkl}, \qquad (4)$$

where, $f = 1/2[(\rho/\rho_0)^{2/3} - 1]$ is the Eulerian finite strain, C^0_{ijkl} is the value of elastic constant at ambient conditions, $\Delta_{ijkl} = -\delta_{ij}\delta_{kl} - \delta_{ik}\delta_{jl} - \delta_{il}\delta_{jk}$, and P is pressure. $a_1 = 3K_{0T}(\partial C^0_{ijkl}/\partial P + \Delta_{ijkl}) - 7C^0_{ijkl}$, and $\partial C^0_{ijkl}/\partial P$ is the pressure derivative of the elastic constant at ambient conditions. The relation between the full notation of C_{ijkl} and its contracted notation C_{ij} is:

ij, kl	11	22	33	23, 32	31, 13	12, 21
i, j	1	2	3	4	5	6

[15] The fitted values of individual elastic constants, aggregate moduli, and their pressure derivatives are reported in Tables 4–7 together with values from the literature. Figures 3–6 show the plots of elastic constants, and aggregate moduli as a function of pressure. The individual elastic constants and aggregate moduli for grossular-rich and almandine rich garnets define nearly linear trends with pressure. The elastic anisotropy of a cubic material can be described by the anisotropy factor, $A = 2C_{44}/(C_{11}-C_{12})$, where A = 1 corresponds to elastic isotropy. The almandine-rich garnet has very low anisotropy (anisotropy factor, A = 0.98) and becomes only slightly more anisotropic with pressure (A = 0.96 at 12.0 GPa). The grossular garnet also has relatively low anisotropy (A = 0.89) at ambient conditions and the anisotropy increases in magnitude modestly (A = 0.84) at the highest pressure. Increasing temperature decreases the elastic anisotropy of garnets [*Isaak et al.*, 1992], and so under upper mantle conditions the elastic anisotropy of garnets should be small and close to that at ambient conditions. For comparison, the ambient pressure anisotropy factor for other cubic minerals

Table 6. Individual Elastic Constants and Pressure Derivatives of Almandine-Rich Garnet at Ambient Conditions[a]

Study[b]	Composition	C_{11}, GPa	C_{12}, GPa	C_{44}, GPa	$(\partial C_{11}/\partial P)_0$	$(\partial C_{12}/\partial P)_0$	$(\partial C_{44}/\partial P)_0$	P_{max}, GPa
a	$Alm_{72}Pyp_{20}Sps_3Grs_3And_2$	304.4(18)	110.3(15)	94.6(5)	6.6(3)	3.6(2)	1.3(1)	12
b	$Alm_{81}Pyp_{14}Grs_4Sps_1$	304.8	112.3	94.4				10^{-4}
c	$Alm_{46}Sps_{54}$	308.5	112.3	94.8	7.15	3.85	1.29	0.5
d	$Alm_{76}Pyp_{21}Grs_3$	306.2	112.5	92.7	7.48	4.41	1.31	0.3
e	$Alm_{52}Sps_{46}Grs_1$	306.5	111.2	94.4	6.69	3.54	1.26	1

[a]Numbers in parentheses are 1-σ deviations in last digit.
[b]Studies are as follows: a, this study; b, *Verma* [1960]; c, *Wang and Simmons* [1974]; d, *Soga* [1967]; e, *Isaak and Graham* [1976].

Table 7. Aggregated Moduli and Pressure Derivatives of Almandine-Rich Garnet at Ambient Conditions[a]

Study[b]	Composition	K_{S0}, GPa	K_{T0}, GPa	G_0, GPa	$(\partial K_S/\partial P)_{T0}$	$(\partial K_T/\partial P)_{T0}$	$(\partial G/\partial P)_0$	P_{max}, GPa	Method[c]
a	$Alm_{72}Pyp_{20}Sps_3Grs_3And_2$	174.9(16)	173.6(16)	95.6(5)	4.7(3)	4.7(3)	1.4(1)	12	BS
b	$Alm_{81}Pyp_{14}Grs_4Sps_1$	176.5		95.1				10^{-4}	U^S
c	$Alm_{46}Sps_{54}$	177.7		96.1	4.95		1.44	0.5	U^S
d	$Alm_{76}Pyp_{21}Grs_3$	177		94	5.43		1.40	0.3	U^S
e	$Alm_{52}Sps_{46}Grs_1$	176.3		95.6	4.59			1	U^S
f	$Alm_{73}Pyp_{27}$	175		99				10^{-4}	U^S
g	Alm_{100}	175.1(9)		92.1	6.2(5)		1.6(2)	3	U^P
h	$Alm_{76}Pyp_{21}Grs_3$[d]		173(6)			5.4[e]		26	X
h	Alm_{100}		168(5)			5.4[e]		26	X
i	Alm_{100}		175(7)			1.5(1.6)		10	X
j	Alm_{100}		178[e]			4.9(1)		21	X

[a]Numbers in parentheses are 1-σ deviations in last digit.
[b]Studies are as follows: a, this study; b, *Verma* [1960]; c, *Wang and Simmons* [1974]; d, *Soga* [1967]; e, *Isaak and Graham* [1976]; f, *Chen et al.* [1997]; g, *Wang and Ji* [2001]; h, *Takahashi and Liu* [1970]; i, *Sato et al.* [1978]; j, *Zhang et al.* [1999].
[c]BS, Brillouin scattering; U^S, single crystal ultrasonic method; U^P, polycrystalline ultrasonic method; X, X-ray diffraction.
[d]Same sample as in d.
[e]Fixed value.

such as MgO is 1.53 [*Sinogeikin and Bass*, 2000] and $MgAl_2O_4$ is 2.46 [*Suzuki et al.*, 2000].

[16] For our grossular-rich garnet, $Grs_{87}And_9Pyp_2Alm_1$, the fit value of the adiabatic bulk modulus K_{S0} at ambient condition is 165.0 ± 0.9 GPa, which is about 3 GPa lower than previous values for grossular garnets [*Bass*, 1989; *Isaak et al.*, 1992]. Assuming a linear dependence of the elastic moduli on composition expressed in mole fraction of the end members, correcting for the larger andradite content of our sample reduces this difference by about 1 GPa. For the shear modulus, our value also remains 1.4–3.0 GPa below the other studies after correction for andradite content. This level of uncertainty (∼1–3%) is typical of those found when comparing multiple measurements on the same or similar compositions for minerals such as fayalite [*Isaak et al.*, 1993] and fluorite [*Speziale and Duffy*, 2002]. We note that the RMS deviations for the Brillouin measurements of *Bass* [1989] are about 50% larger than this study.

[17] The fit values of K'_{T0} and G'_0 of grossular are 3.9 ± 0.2 and 1.1 ± 0.1 and are compared with previous values in Table 5. *Conrad et al.* [1999] reported a Brillouin scattering study on grossular, andradite, and pyrope at high pressures using a very similar experimental technique as this study. In previous work [*Jiang et al.*, 2004], we found large discrepancies between our results and those of *Conrad et al.* [1999] for andradite. For grossular, while the pressure derivative of the shear modulus is in excellent agreement, we obtain a much lower value for K'_{S0}. *Conrad et al.* [1999] measured two crystal directions at each pressure compared with 36 in this study. The large differences may result from orientation errors in the previous study.

[18] The high-pressure X-ray diffraction studies listed in Table 5 report a wide range of pressure derivatives. The determination of the bulk modulus and its pressure derivative from static compression relies on fits to the slope of the measured P-V curve, and hence is less direct than Brillouin scattering measurements. Static compression studies also suffer from a well-known tradeoff between fit values for K_{T0} and K'_{T0}. Furthermore, if measurements are restricted to purely hydrostatic conditions, the compression range is very limited making it difficult to constrain the elastic moduli. On the other hand, data which covers a broad pressure range are subjected to variable degrees of nonhydrostatic stress depending on the nature and amount of the pressure transmitting medium. Figure 7 shows a comparison of the pressure-compression curve from our Brillouin data with previous X-ray diffraction studies. Below ∼8 GPa, our

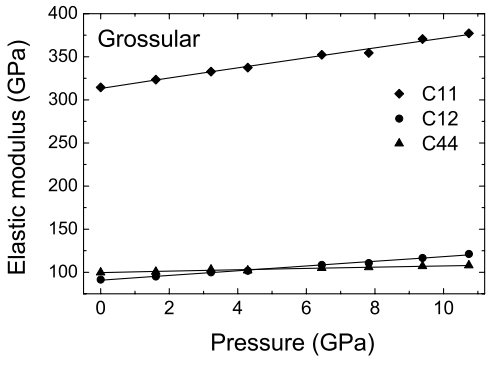

Figure 3. Pressure dependencies of the elastic stiffness constants for grossular-rich garnet; solid lines are fits using Eulerian finite strain equations.

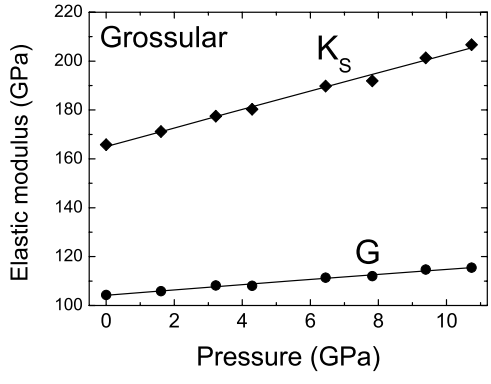

Figure 4. Grossular aggregate adiabatic bulk modulus K_S and G (symbols) and fits (lines) to Eulerian finite strain equations.

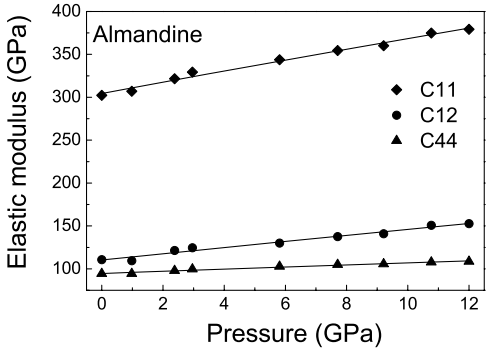

Figure 5. Pressure dependencies of the elastic stiffness constants C_{ij} for natural almandine garnet; solid lines are fits using Eulerian finite strain equations.

results are in very good agreement with earlier studies. The results of *Pavese et al.* [2001] and *Zhang et al.* [1999] indicated that their samples became increasingly less compressible than ours at higher pressures above 8 GPa. *Olijnyk et al.* [1991] performed compression studies on a synthetic grossular using both methanol-ethanol (M-E) and N_2 as pressure transmitting media. Their P-V curve obtained using M-E as pressure medium is in very good agreement with ours to 10 GPa, while their P-V curve above 9 GPa derived using N_2 as pressure medium deviates from ours. The methanol-ethanol mixture remains strictly hydrostatic up to 12 GPa, while N_2 and Ne freeze above 3 GPa and 4.5 GPa, respectively, and generate nonhydrostatic stress conditions at higher pressures.

[19] For almandine-rich garnet $Alm_{72}Pyp_{20}Sps_3Grs_3And_2$, both individual elastic constants C_{ij}, aggregate moduli K_{S0} and G_0 are in agreement (Tables 6 and 7) with those of a natural almandine with very similar composition $Alm_{76}Pyp_{21}Grs_3$ [*Soga*, 1967], and they also agree well with other reported values (Table 7) after correcting for compositional differences. In general, there is a good agreement among various studies for $\partial C_{44}/\partial P$ and $(\partial G/\partial P)$. However, there is a wide range of reported values for the pressure derivatives of C_{11}, C_{12}, and K_{S0}. Our result for K'_{S0} is consistent with the low-end values of the range for K'_{S0} in previous ultrasonic studies.

[20] A comparison of the isothermal compression curve derived from the Brillouin measurements with static X-ray

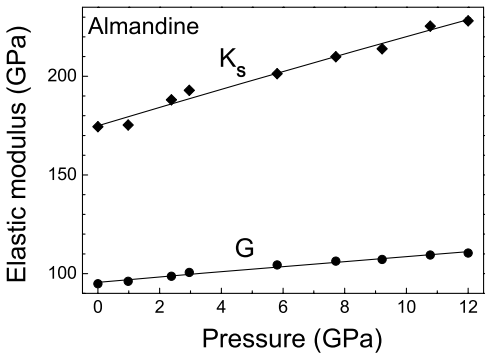

Figure 6. Almandine aggregate adiabatic bulk modulus K_S and G (symbols) and fits (lines) using Eulerian finite strain equations.

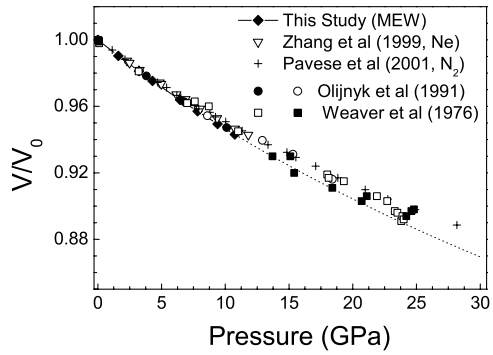

Figure 7. Isothermal compression curve of grossular calculated from present study (solid line) and its extrapolation to higher pressures (dotted line). Previous compression studies of X-ray diffraction are plotted together for comparison. Filled and open circles are from the work of *Olijnyk et al.* [1991] using M-E and N_2 as pressure medium, respectively. From the work of *Weaver et al.* [1976], open squares are 90% Grs, filled squares are 98% Grs, and the pressure medium is NaCl.

diffraction data is shown in Figure 8. As with almandine, our compression curve agrees well with earlier compression studies at low pressure, and is also consistent until 10 GPa with data obtained using M-E as pressure transmitting medium [*Sato et al.*, 1978]. Compression curves using Ne and He pressure medium [*Zhang et al.*, 1999] deviate from ours above 6 GPa and 11 GPa, respectively. It is somewhat surprising (Figure 8) that X-ray data obtained with a He medium yields a similar compression curve to those obtained using Ne and NaCl since helium is expected to provide the closest approach to hydrostaticity. However, deviations from the hydrostatic compression curve can result for any pressure medium if an insufficient

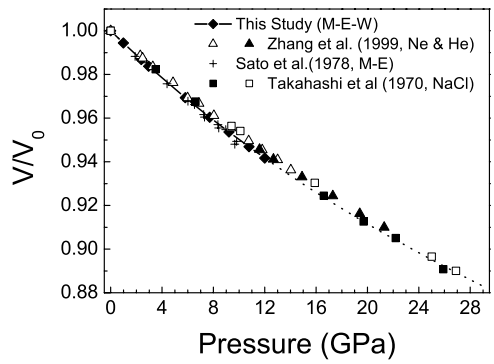

Figure 8. Isothermal compression curve of almandine calculated from the present study (solid line) and its extrapolation to higher pressures (dotted line). Previous compression studies of X-ray diffraction are plotted together for comparison. From the work of *Zhang et al.* [1999], open triangles are Ne as pressure medium and filled triangles are He as pressure medium. From the work of *Takahashi and Liu* [1970], NaCl is the pressure medium, open squares are natural almandine, and filled squares are synthetic almandine.

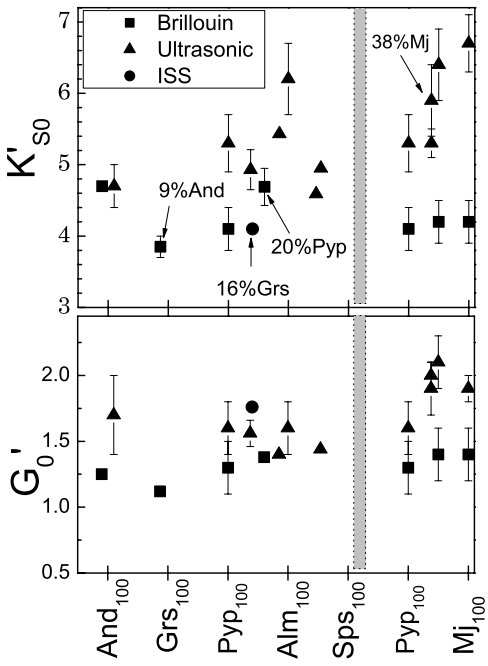

Figure 9. (left) Pressure derivatives K'_{S0} and G'_0 of various garnets obtained by Brillouin scattering, impulsively stimulated scattering (ISS), and ultrasonic methods. (right) Pressure derivatives of pyrope-majorite compositions. References are as follows: for Brillouin, this study, *Jiang et al.* [2004], and *Sinogeikin and Bass* [2000, 2002]; for ISS, *Chai et al.* [1997]; for ultrasonic, *Chen et al.* [1999], *Isaak and Graham* [1976], *Soga* [1967], *Wang and Ji* [2001], *Wang and Simmons* [1974], *Liu et al.* [2000], *Rigden et al.* [1994], *Gwanmesia et al.* [1998], and *Webb* [1989]. Values of K'_{S0} for andradite and values of G'_0 for pyrope-almandine have been offset slightly in composition for clarity.

amount of the medium is loaded together with the sample, resulting in partial bridging and generation of deviatoric stresses. The large range of K_{T0} and especially K'_{T0} values reported for X-ray studies in Tables 5 and 7 despite relatively modest differences in pressure-volume behavior exhibited in Figures 7 and 8 demonstrates the difficulty in reliably constraining these parameters from X-ray diffraction data.

4.2. Implications for High-Pressure Elasticity of Garnets

[21] In general, ambient pressure elastic moduli determined by different techniques are in reasonable agreement (see Tables 5 and 7), but the pressure derivatives are highly discrepant as seen in Figure 9. Compression studies using X-ray diffraction can not give information about G and its pressure derivative, and provide less reliable value for K_{T0} and K'_{T0} because of parameter tradeoffs and nonhydrostatic stresses as discussed above. Ultrasonic methods provide a direct measurement of elasticity and acoustic velocities through travel time measurements, but are subject to uncertainties when polycrystalline samples are used, especially when combined with a limited pressure range [e.g., *Wang and Ji*, 2001]. The presence of pores and cracks in the sample could lead to an overestimate of pressure derivatives. Single-crystal ultrasonic studies were instead generally limited to very low pressures (<3 GPa). If the precision is adequate, slopes at lower pressures can be well constrained, but may not be applicable to higher pressures. Figure 9 shows pressure derivatives of garnets measured by Brillouin and ultrasonic methods. It is evident that pressure derivatives derived by ultrasonic methods are more scattered and in general higher than those by Brillouin scattering. The results of *Conrad et al.* [1999] probably suffered systematic errors, as discussed above and are not included. Brillouin scattering has advantages over other methods in that measurements on a large number of directions on high-quality single crystals can be performed under strictly hydrostatic conditions.

[22] The aggregate elastic properties of garnets at high pressures have also been investigated theoretically using density functional theory [*Akhmatskaya et al.*, 1999]. The pressure derivatives of the bulk modulus obtained theoretically for grossular (K_{T0} = 166 GPa, K'_{T0} = 4.3) and almandine (K_{T0} = 177 GPa, K'_{T0} = 4.2) are within ~10% of the experimental values obtained here (which is the expected accuracy of the DFT calculations [*Milman et al.*, 2001]). The theoretical values for pyrope (K_{T0} = 170 GPa, K'_{T0} = 4.3) are also consistent with spectroscopic measurements [*Sinogeikin and Bass*, 2000] (Figure 9) rather than the higher values reported in ultrasonic studies. A related theoretical study [*Milman et al.*, 2001] reported values for the bulk modulus and pressure derivative of andradite (K_{T0} = 147 GPa, K'_{T0} = 4.4) that are 5~7% lower than recent Brillouin scattering results [*Jiang et al.*, 2004]. Nevertheless, it is notable that these theoretical studies yield bulk modulus pressure derivatives in the range of 3.9–4.8 over a wide range of garnet compositions, consistent with the overall range reported in optical spectroscopic determinations (Table 8) and considerably lower than the upper range of values reported in static compression and ultrasonic studies.

Table 8. End-Member Aggregate Elastic Properties of Garnets From Spectroscopic (Brillouin) Data[a]

	Formula	a (Å)	K_{S0} (GPa)	G_0 (GPa)	$(\partial K_S/\partial P)_{T0}$	$(\partial G/\partial P)_0$	Reference[b]
Almandine	$Fe_3Al_2Si_3O_{12}$	11.531	175(2)	96(1)	4.9(2)	1.4(1)	a
Pyrope	$Mg_3Al_2Si_3O_{12}$	11.452	171(3)	94(2)	4.1(3)	1.3(2)	b
Grossular	$Ca_3Al_2Si_3O_{12}$	11.845	168(1)	109(4)	3.9(2)	1.1(1)	a
Andradite	$Ca_3Fe_2Si_3O_{12}$	12.058	157(2)	90(1)	4.7(1)	1.3(1)	c
Majorite	$Mg_4Si_4O_{12}$	11.494	166(3)	85(2)	4.2(3)	1.4(2)	d

[a]Lattice parameters from *Smyth and McCormick* [1995].
[b]References are as follows: a, this study, extrapolated to end-member composition using a linear mixing model; b, *Sinogeikin and Bass* [2000]; c, *Jiang et al.* [2004]; d, *Sinogeikin and Bass* [2002].

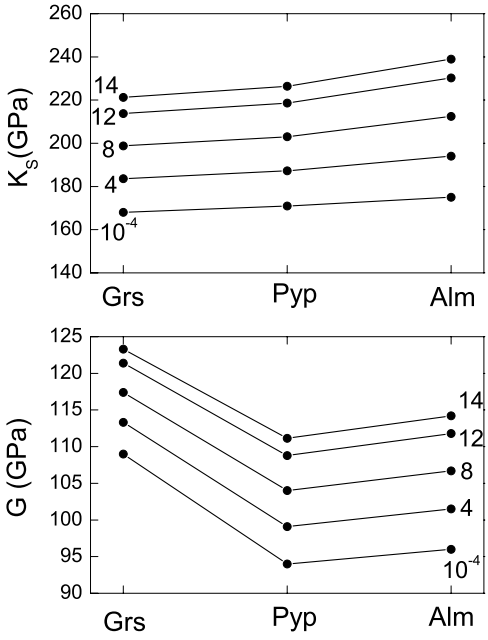

Figure 10. Bulk and shear moduli versus composition for the pyrope-almandine series and the pyrope-grossular series at selected pressures from 1 bar to 14 GPa using the data of Table 8. Numbers next to each line are pressures in GPa.

[23] Table 8 provides values for the aggregate elastic moduli of end-member garnets derived from this work and other Brillouin scattering studies [*Bass*, 1989; *Sinogeikin and Bass*, 2000, 2002; *Chai et al.*, 1997; *Jiang et al.*, 2004]. No compositional trends are evident in the pressure derivatives except for an increase in K'_{S0} upon substitution of Fe^{2+} for Mg^{2+} in the pyrope-almandine series and a similar increase in K'_{S0} upon substitution of Fe^{3+} for Al^{3+} in the grossular-andradite series. The value of K'_{S0} for pure almandine has been extrapolated from our measured value assuming a linear dependence on mole fraction. It is notable that a similar increase in K'_{S0} with Fe^{2+}-Mg^{2+} substitution was observed for the forsterite-fayalite series (S. Speziale et al., manuscript in preparation, 2004).

[24] Figure 10 shows the bulk and shear moduli versus composition for the pyrope-almandine series and the pyrope-grossular series at selected pressures from 0 to 14 GPa using the data of Table 8 and assuming a linear dependence of both moduli and their pressure derivatives on composition expressed in mole fraction of the end members. At ambient pressure, the bulk modulus varies by ~2% across the pyrope-grossular and pyrope-almandine systems. Owing to the higher K'_{S0} value for almandine, the increase in bulk modulus from pyrope to garnet becomes 5.2% by 14 GPa. Ca^{2+}-Mg^{2+} substitution has a large effect on the shear modulus: the rigidity of grossular is 16% greater than pyrope at ambient pressure. This is mostly maintained across the upper mantle pressure interval as the shear modulus of grossular is 11% greater than pyrope at 14 GPa. In contrast to other silicates such as olivine, the effect of Fe^{2+}-Mg^{2+} is modest for garnets. The shear modulus of almandine is 2–3% larger than that of pyrope at 0–14 GPa. The implications of these results for assessing compositional variation in the upper mantle will be the subject of a forthcoming publication.

5. Conclusions

[25] Brillouin scattering measurements have been carried out under hydrostatic conditions to 11 GPa on a grossular-rich and an almandine-rich garnet. Individual, and aggregate elastic moduli, and their pressure derivatives have been determined by fitting Eulerian finite strain equations. All the elastic constants, and aggregate moduli define nearly linear trends with pressure. The adiabatic bulk, and Voigt-Reuss-Hill average shear moduli and their pressure derivatives were constrained to K_{S0} = 165.0 ± 0.9 GPa, G_0 = 104.2 ± 0.3 GPa, K'_{S0} = 3.8 ± 0.2 and G'_0 = 1.1 ± 0.1 for the grossular-rich garnet and K_{S0} = 174.9 ± 1.6 GPa, G_0 = 95.6 ± 0.5 GPa, K'_{S0} = 4.7 ± 0.3 and G'_0 = 1.4 ± 0.1 for the almandine-rich garnet.

[26] A compression curve derived from our results is in good agreement with high-pressure X-ray diffraction data, especially those data recorded under hydrostatic conditions. Elasticity data for almandine- and grossular-rich garnets were compiled and evaluated. The ambient pressure moduli show good agreement but reported pressure derivatives exhibit wide variations that show little correlation with composition, but rather appear to be related to experimental technique. By restricting attention to high-pressure optical spectroscopy (Brillouin scattering) studies, a set of self-consistent aggregate elastic properties and their pressure derivatives were derived for the major upper mantle garnet end-member compositions.

[27] These results (Table 8) demonstrate that pressure derivatives of elastic moduli for mantle-relevant garnets fall in a relatively narrow range and are considerably lower than inferred from some earlier studies. Several recent mineralogical models for the upper mantle [*Goes et al.*, 2000; *Cammarano et al.*, 2003; *Lee*, 2003] have adopted elastic properties for garnets, especially grossular garnets and Mg-rich majorites outside the range of the optical spectroscopic data set. Our development of an experimentally consistent data set of end-member garnet properties will result in improved mineralogical models for the mantle, and also allow better constraints on the lateral variation of seismic velocities due to local chemical variations in the mantle.

[28] **Acknowledgments.** This work was supported by the National Science Foundation and the David and Lucile Packard Foundation. We are grateful to J. Delaney, Rutgers University, for the microprobe analysis.

References

Akhmatskaya, E. V., R. H. Nobes, V. Milman, and B. Winkler (1999), Structural properties of garnets under pressure: An ab initio study, *Zeitschr. Kristallogr.*, *214*, 808–819.

Babuska, V., J. Fiala, M. Kumazawa, I. Ohno, and Y. Sumino (1978), Elastic properties of garnet solid solution series, *Phys. Earth Planet. Inter.*, *16*, 157–176.

Bass, J. D. (1986), Elasticity of uvarovite and andradite garnets, *J. Geophys. Res.*, *91*, 7505–7516.

Bass, J. D. (1989), Elasticity of grossular and spessartite garnets by Brillouin spectroscopy, *J. Geophys. Res.*, *94*, 7621–7628.

Birch, F. (1978), Finite strain isotherm and velocities for single-crystal and polycrystalline NaCl at high pressures and 300 K, *J. Geophys. Res.*, *83*, 1257–1264.

Cammarano, F., S. Goes, P. Vacher, and D. Giardini (2003), Inferring upper-mantle temperatures from seismic velocities, *Phys. Earth Planet. Inter.*, *138*, 197–222.

Chai, M., J. M. Brown, and L. J. Slutsky (1997), The elastic constants of a pyrope-grossular-almandine garnets to 20 GPa, *Geophys. Res. Lett.*, *24*, 523–526.

Chen, G., R. Miletich, C. Mueller, and H. A. Spetzler (1997), Shear and compressional mode measurements with GHz ultrasonic interferometry and velocity-composition systematics for the pyrope-almandine solid solution series, *Phys. Earth Planet. Inter.*, *99*, 273–287.

Chen, G., J. A. Cooke, G. D. Gwanmesia, and R. C. Liebermann (1999), Elastic wave velocities of $Mg_3Al_2Si_3O_{12}$-pyrope garnet to 10 GPa, *Am. Mineral.*, *84*, 384–388.

Conrad, P. G., C.-S. Zha, H.-K. Mao, and R. J. Hemley (1999), The high-pressure, single-crystal elasticity of pyrope, grossular, and andradite, *Am. Mineral.*, *84*, 374–383.

Davies, G. F. (1974), Effective elastic moduli under hydrostatic stress, I, Quasi-harmonic theory, *J. Phys. Chem. Solids*, *35*, 1513–1520.

Duffy, T. S., and D. L. Anderson (1989), Seismic velocities in mantle minerals and the mineralogy of the upper mantle, *J. Geophys. Res.*, *94*, 1895–1912.

Every, A. G. (1980), General closed-form expressions for acoustic waves in elastically anisotropic solids, *Phys. Rev. B*, *22*, 1746–1760.

Fei, Y., and C. M. Bertka (1999), Phase transitions in the Earth's mantle and mantle mineralogy, in *Mantle Petrology: Field Observations and High Pressure Experimentation*, *Spec. Publ.*, vol. 6, edited by Y. Fei, C. M. Bertka, and B. O. Mysen, pp. 189–207, Geochem. Soc., Houston, Tex.

Forte, A. M., and H. K. C. Perry (2000), Geodynamic evidence for a chemically depleted continental tectosphere, *Science*, *290*, 1940–1944.

Goes, S., R. Govers, and P. Vacher (2000), Shallow mantle temperatures under Europe from *P* and *S* wave tomography, *J. Geophys. Res.*, *105*, 11,153–11,169.

Gwanmesia, G. D., G. Chen, and R. C. Liebermann (1998), Sound velocities in $MgSiO_3$-garnet to 8 GPa, *Geophys. Res. Lett.*, *25*, 4553–4556.

Irifune, T., and A. E. Ringwood (1993), Phase transformations in subducted oceanic crust and buoyancy relationships at depths of 600–800 km in the mantle, *Earth Planet. Sci. Lett.*, *117*, 101–110.

Isaak, D. G., and E. K. Graham (1976), The elastic properties of an almandine-spessartine garnet and elasticity in the garnet solid solution series, *J. Geophys. Res.*, *81*, 2483–2489.

Isaak, D. G., O. L. Anderson, and H. Oda (1992), High-temperature thermal expansion and elasticity of calcium-rich garnets, *Phys. Chem. Min.*, *19*, 106–120.

Isaak, D. G., E. K. Graham, J. D. Bass, and H. Wang (1993), The elastic properties of single-crystal fayalite as determined by dynamical measurement techniques, *Pure Appl. Geophys.*, *141*, 393–414.

Jackson, I., R. L. Rudnick, S. Y. Oreilly, and C. Bezant (1990), Measured and calculated elastic wave velocities for xenoliths from the lower crust and upper mantle, *Tectonophysics*, *173*, 207–210.

Jiang, F., S. Speziale, S. R. Shieh, and T. S. Duffy (2004), Single crystal elasticity of andradite garnet to 11 GPa, *J. Phys. Condens. Matter*, *16*, S1041–S1052.

Jordan, T. H. (1978), Composition and development of continental tectosphere, *Nature*, *274*, 544–548.

Karato, S., and B. B. Karki (2001), Origin of lateral variation of seismic wave velocities and density in the deep mantle, *J. Geophys. Res.*, *106*, 21,771–21,783.

Knittle, E. (1995), Static compression measurements of equations of state, in *A Handbook of Physical Constants: Mineral Physics and Crystallography*, *AGU Ref. Shelf*, vol. 2, edited by T. J. Ahrens, pp. 98–142, AGU, Washington, D. C.

Lee, C.-T. A. (2003), Compositional variation of density and seismic velocities in natural peridotites at STP conditions: Implications for seismic imaging of compositional heterogeneities in the upper mantle, *J. Geophys. Res.*, *108*(B9), 2441, doi:10.1029/2003JB002413.

Liu, J., G. Chen, G. D. Gwanmesia, and R. C. Liebermann (2000), Elastic wave velocities of pyrope-majorite garnets ($Py_{62}Mj_{38}$ and $Py_{50}Mj_{50}$) to 9 GPa, *Phys. Earth Planet. Inter.*, *120*, 153–163.

Mao, H. K., J. Xu, and P. M. Bell (1986), Calibration of the ruby pressure gauge to 800 kbar under quasi-hydrostatic conditions, *J. Geophys. Res.*, *91*, 4673–4676.

Milman, V., E. V. Akhmatskaya, R. H. Nobes, B. Winkler, C. J. Pickard, and J. A. White (2001), Systematic ab initio study of the compressibility of silicate garnets, *Acta Crystallogr., Sect. B Struct. Sci.*, *57*, 163–177.

Morozov, I. B., N. I. Christensen, S. B. Smithson, and L. S. Hollister (2003), Seismic and laboratory constraints on crustal formation in a former continental arc (Accrete, southeastern Alaska and western British Columbia), *J. Geophys. Res.*, *108*(B1), 2041, doi:10.1029/2001JB001740.

Olijnyk, H., E. Paris, C. A. Geiger, and G. A. Lager (1991), Compressional study of katoite $[Ca_3Al_2(O_4H_4)_3]$ and grossular garnet, *J. Geophys. Res.*, *96*, 14,313–14,318.

O'Neill, B., J. D. Bass, J. R. Smyth, and M. T. Vaughan (1989), Elasticity of a grossular-pyrope-Almandine garnet, *J. Geophys. Res.*, *94*, 17,819–17,824.

Pavese, A., D. Levy, and V. Pischrdda (2001), Elastic properties of andradite and grossular by synchrotron X-ray diffraction at high pressure conditions, *Eur. J. Mineral.*, *13*, 929–937.

Rickwood, P. C., M. Mathias, and J. C. Siebert (1968), A study of garnets from eclogite and peridotite xenoliths found in kimberlite, *Contrib. Mineral. Petrol.*, *19*, 271–301.

Rigden, S. M., G. D. Gwanmesia, and R. C. Liebermann (1994), Elastic wave velocities of a pyrope-majorite garnet to 3 GPa, *Phys. Earth Planet. Inter.*, *86*, 35–44.

Ringwood, A. E. (1967), The pyroxene-garnet transformation in the Earth's mantle, *Earth Planet. Sci. Lett.*, *2*, 255–263.

Ringwood, A. E. (1991), Phase transformations and their bearing on the constitution and dynamics of the mantle, *Geochim. Cosmochim. Acta*, *55*, 2083–2110.

Sato, Y., M. Akaogi, and S. Akimoto (1978), Hydrostatic compression of the synthetic garnets pyrope and almandine, *J. Geophys. Res.*, *83*, 335–338.

Sinogeikin, S. V., and J. D. Bass (2000), Single-crystal elasticity of pyrope and MgO to 20 GPa by Brillouin scattering in the diamond cell, *Phys. Earth Planet. Inter.*, *120*, 43–62.

Sinogeikin, S. V., and J. D. Bass (2002), Elasticity of Majorite and a Majorite-Pyrope solid solution to high pressure: Implications for the transition zone, *Geophys. Res. Lett.*, *29*(2), 1017, doi:10.1029/2001GL013937.

Skinner, B. J. (1966), Thermal expansion, in *Handbook of Physical Constants*, *Geol. Soc. Am. Mem.*, vol. 97, edited by S. P. Clark Jr., pp. 75–95, Geol. Soc. of Am., New York.

Smyth, J. R., and T. C. McCormick (1995), Crystallographic data for minerals, in *A Handbook of Physical Constants: Mineral Physics and Crystallography*, *AGU Ref. Shelf*, vol. 2, edited by T. J. Ahrens, pp. 1–17, AGU, Washington, D. C.

Soga, N. (1967), Elastic constants of garnet under pressure and temperature, *J. Geophys. Res.*, *72*, 4227–4234.

Speziale, S., and T. S. Duffy (2002), Single-crystal elastic constants of fluorite (CaF_2) to 9.3 GPa, *Phys. Chem. Min.*, *29*, 465–472.

Suzuki, I., I. Ohno, and O. L. Anderson (2000), Harmonic and anharmonic properties of spinel $MgAl_2O_4$, *Am. Mineral.*, *85*, 304–311.

Takahashi, T., and L. Liu (1970), Compression of ferromagnesian garnets and the effect of solid solutions on the bulk modulus, *J. Geophys. Res.*, *75*, 5757–5766.

Verma, R. K. (1960), Elasticity of some high-density crystals, *J. Geophys. Res.*, *65*, 757–766.

Wang, H., and G. Simmons (1974), Elasticity of some mantle crystal structures: 3. Spessartine almandine garnet, *J. Geophys. Res.*, *79*, 2607–2613.

Wang, Z., and S. Ji (2001), Elasticity of six polycrystalline silicate garnets at pressure up to 3.0 GPa, *Am. Mineral.*, *86*, 1209–1218.

Weaver, J. S., T. Takahashi, and J. D. Bass (1976), Isothermal compression of grossular garnets to 250 Kbar and the effect of calcium on the bulk modulus, *J. Geophys. Res.*, *81*, 2475–2482.

Webb, S. (1989), The elasticity of the upper mantle orthosilicates olivine and garnet to 3 GPa, *Phys. Chem. Min.*, *16*, 684–692.

Weidner, D. J., and Y. Wang (2000), Phase transformations: Implications for mantle structure, in *Earth's Deep Interior: Mineral Physics and Tomography From the Atomic to the Global Scale*, *Geophys. Monogr. Ser.*, vol. 117, edited by S. Karato et al., pp. 215–235, AGU, Washington, D. C.

Whitfield, C. H., E. M. Brody, and W. A. Bassett (1976), Elastic moduli of NaCl by Brillouin scattering at high pressure in a diamond cell, *Rev. Sci. Intrum.*, *47*, 942–947.

Zha, C.-S., T. S. Duffy, R. T. Downs, H.-K. Mao, and R. J. Hemley (1996), Sound velocity and elasticity of single-crystal forsterite to 16 GPa, *J. Geophys. Res.*, *101*, 17,535–17,545.

Zhang, L., H. Ahsbahs, A. Kutoglu, and C. A. Geiger (1999), Single-crystal hydrostatic compression of synthetic pyrope, almandine, spessartine, grossular and andradite garnets at high pressures, *Phys. Chem. Min.*, *27*, 52–58.

T. S. Duffy, F. Jiang, and S. Speziale, Department of Geosciences, Princeton University, Princeton, NJ 08544, USA. (duffy@princeton.edu; fuj2@lehigh.edu; speziale@uclink.berkeley.edu)